# Space object imaging through the turbulent atmosphere

**J. R. Fienup**
Environmental Research Institute of Michigan
P. O. Box 8618
Ann Arbor, Michigan 48107

## Abstract

For telescopes operating at optical wavelengths, the turbulence of the atmosphere limits the resolution of space objects to about one second of arc, although the diffraction limit of the largest telescopes is many times as fine. We discuss an image processing technique that uses interferometer data (the modulus of the Fourier transform) to reconstruct diffraction limited images. Data from a stellar speckle interferometer or from an amplitude interferometer can be used. The processing technique is an iterative method that finds a real, non-negative object that agrees with the Fourier modulus data. For complicated two-dimensional objects, the solutions found by this technique are surprisingly unique. New results are shown for simulated speckle interferometer data having realistic noise present.

## I. Introduction

The aim of the research described here is to develop a new method of recovering imagery through the turbulent atmosphere. Ordinarily, atmospheric turbulence limits the resolution of an image obtained through a large telescope. Under good "seeing" conditions, the atmospheric resolution limit is typically one second of arc, which is the diffraction limit of an optical telescope of aperture 10 cm. Thus, the turbulent atmosphere limits the resolution of imagery obtained through a five-meter telescope to 1/50 the resolution of which it would otherwise be capable.

A number of interferometric techniques,[1] including the intensity interferometer of Hanbury Brown and Twiss,[2] the speckle interferometer of Labeyrie,[3] and the amplitude interferometer of Currie,[4] have been developed for obtaining diffraction-limited information about the modulus of the Fourier transform of the object. The autocorrelation of the object can be computed from the Fourier modulus, allowing the diameter of the object to be determined. However, without knowledge of the Fourier transform phase, the object itself generally cannot be computed except for the special cases of objects with nearby isolated point sources or objects known to be centro-symmetric. This is known as the phase problem of optical coherence theory.

Previous attempts at reconstructing an object from the modulus of its Fourier transform[5-9] have not proven to be practical for complicated two-dimensional imagery. We describe in this paper a new method[10] for reconstructing an object from its Fourier modulus which *is* practical for complicated two-dimensional imagery, even when a considerable amount of noise is present in the Fourier modulus data. In addition, we will show preliminary experimental results using data that is a realistic simulation of a speckle interferometer process, including the effects of atmospheric turbulence, a finite number of short-exposure images, an imperfect compensation for the MTF of the system, and multiplicative photon noise. These preliminary results indicate that, using this reconstruction method with speckle data, we can realistically expect to reconstruct images with resolution many times better than what is ordinarily allowed by the turbulent atmosphere.

The reconstruction method, which is iterative and relies only on the Fourier modulus and the non-negativity of the object, is described in Section II of this paper. In Section III, experimental results will be shown for the case of ideal noise-free Fourier modulus data. In Section IV is described the computer simulation of the speckle interferometer process, and the noise characteristics of that data are discussed in Section V. The reconstruction results using the simulated speckle data are shown in Section VI.

## II. Description of the Method

Let the two-dimensional sky-brightness function which we wish to image be f(x, y). Its Fourier transform is

$$F(u, v) = |F(u, v)| \exp [i\theta(u, v)] = \mathcal{F}\{f(x, y)\}$$

$$= \iint_{-\infty}^{\infty} f(x, y) \exp [-i2\pi(ux + vy)]\, dx\, dy \qquad (1)$$

where (x, y) are spatial (or angular) coordinates and (u, v) are spatial (or angular) frequencies. f(x, y) is a real, non-negative function and F(u, v) is complex valued and hermetian. It is assumed that only |F(u, v)| is measured. The diameter of the object can be computed, since it is just half the diameter of the autocorrelation, $f \star f = \mathcal{F}\{|F(u, v)|^2\}$.

The mathematical problem to be solved is the following: find a Fourier transform pair $G(u, v) = \mathcal{F}\{g(x, y)\}$ that satisfies all the known constraints: the Fourier-domain constraint that |G(u, v)| equals the measured Fourier modulus, and the object- (or image-) domain constraint that g(x, y) be non-negative. An auxiliary object-domain constraint is that the diameter of the object be half the diameter of the autocorrelation. Although it is not necessary to impose this diameter constraint (since it follows directly from the knowledge of the Fourier modulus and the object's non-negativity), it can be useful for finding solutions. If such a Fourier transform pair is found, then a possible solution has been found to the physical problem: what physical object could give rise to the measured data. Unfortunately, it may be that many different objects could give rise to the same Fourier modulus data; however, as will be discussed later, we have not found the question of

#5011 received Dec. 18, 1978. This paper was presented at the SPIE seminar on Applications of Digital Image Processing, August 28–29, 1978, San Diego, and appears in SPIE Proceedings Vol. 149.

uniqueness to be a problem for complicated two-dimensional images.

The new approach to determining an object from the modulus of its Fourier transform is a modification of an iterative approach originally used by Gerchberg and Saxton to solve a problem in electron microscopy,[11] and later by others in connection with computer-generated holograms.[12-14] We first modified the Gerchberg-Saxton algorithm to fit this problem simply by using the object constraints discussed above. We refer to this algorithm as the error-reduction approach. We also modified the algorithm in a fundamental way to arrive at the more powerful input-output approach.

In the error-reduction approach, one iteratively transforms back and forth between the Fourier and object domains, imposing the constraints in each domain before returning to the other domain (as indicated in Figure 1), seeking to find a solution that satisfies the constraints in both domains. In the Fourier domain,

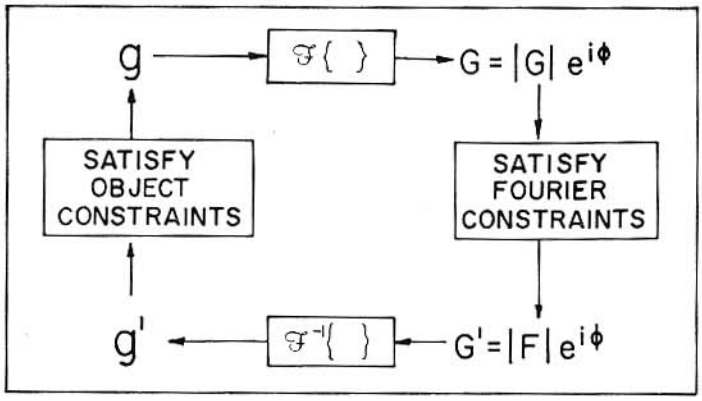


**Figure 1. Block diagram of the error-reduction approach.**

$G'(u, v)$ is formed by replacing the modulus of $G(u, v)$ with the measured modulus, $|F(u, v)|$. In the object domain, $g(x, y)$ is formed by setting $g'(x, y) = 0$ where it violates the constraints. The iterations can be initialized in a number of different ways, for example, by using a sequence of random numbers either for $g(x, y)$, the estimate of the object, or for $\phi(u, v)$, the estimate of the Fourier transform phase.

The mean-squared error at each iteration can be defined in the Fourier domain by

$$E_F^2 = \frac{\displaystyle\iint_{-\infty}^{\infty} [|G(u, v)| - |F(u, v)|]^2 \, du \, dv}{\displaystyle\iint_{-\infty}^{\infty} |F(u, v)|^2 \, du \, dv} \tag{2}$$

or in the object domain by

$$E_o^2 = \frac{\displaystyle\iint_{\gamma} [g'(x, y)]^2 \, dx \, dy}{\displaystyle\iint_{-\infty}^{\infty} [g'(x, y)]^2 \, dx \, dy} \tag{3}$$

where $\gamma$ includes all points at which $g'(x, y)$ violates the constraints. It can be shown that the mean-squared error can only decrease (or at least not increase) at each iteration, giving rise to the name error-reduction approach. However, although the mean-squared error decreases rapidly for the first few iterations, it decreases extremely slowly for later iterations.[11,12] For the present application, the error-reduction approach requires an impractically large number of iterations for convergence.

During an attempt to alter the algorithm in order to achieve a more rapid decrease of the error, a new and more powerful approach was developed: the input-output approach.[13,14] The first three operations of the input-output approach are the same as those of the error-reduction approach: $g(x, y)$ is Fourier transformed, the transform modulus is made equal to the measured Fourier modulus, and the result is inverse-Fourier transformed, giving the image $g'(x, y)$. Together, those three operations can be viewed as a nonlinear system having an input $g(x, y)$ and an output $g'(x, y)$, as depicted in Figure 2. A

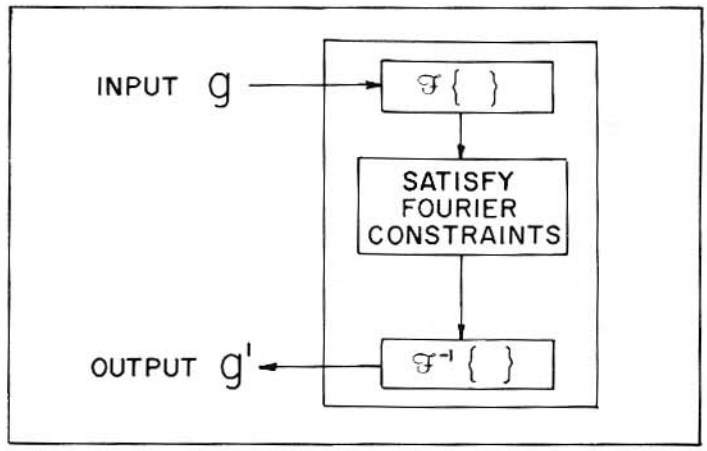


**Figure 2. Block diagram of the system for the input-output concept.**

characteristic of this system is that the output, $g'(x, y)$, has a Fourier transform having a modulus equal to $|F(u, v)|$. Therefore, if we can manipulate the input in such a way as to force the output to be non-negative, then the output is a solution to our problem. The new input is not necessarily a modified version of the previous output, nor does it have to satisfy the constraints: rather, it is the driving function for the next output.

For a previous application, analysis was performed to determine what effect a change in the input would have on the output. Suppose that at the $k^{th}$ iteration, the input $g_k(x, y)$ results in the output $g'_k(x, y)$. Then at the next iteration, the input is

$$g_{k+1}(x, y) = g_k(x, y) + \Delta g(x, y) \tag{4}$$

which results in the output

$$g'_{k+1}(x, y) = g'_k(x, y) + \Delta g'(x, y) \tag{5}$$

The result of the analysis[14] is that the expected change in the output is approximately given by

$$E[\Delta g'(x, y)] = \alpha \Delta g(x, y) \tag{6}$$

where $E[\cdot]$ is the expected, or mean, value and $\alpha$ depends on the statistics of $|G(u, v)|$ and $|F(u, v)|$. [$\Delta g'(x, y)$ also has a non-zero variance; that is, its value cannot be exactly predicted.] Thus, if, in order to drive the output to satisfy the constraints, we desire the change in the output to be $\Delta g_d(x, y)$, then a good choice of the change in the input would be $\alpha^{-1}\Delta g_d(x, y)$.

As shown in Ref. 14, despite the fact that there is no guarantee that the error will decrease on each iteration, the approach has been very successful and is superior to the error-reduction approach. The input-output method allows for considerable flexibility and inventiveness in the selection of the next input. The error-reduction approach can be thought of as just one of the alternatives allowed in the more general input-output approach.

As was the case for the previous applications, there are a number of different methods of choosing $g_{k+1}(x, y)$, given $g_k'(x, y)$ and $g_k(x, y)$, based on different points of view and different

tradeoffs inherent in the input-output approach. A particularly successful method of choosing the next input is given by

$$g_{k+1}(x, y) = \begin{cases} g'_k(x, y), & (x, y)\varepsilon\gamma \\ g_k(x, y) - \beta g'_k(x, y), & (x, y)\varepsilon\gamma \end{cases} \quad (7)$$

where $\gamma$ is defined as in Eq. (3), and $\beta$ is a constant. In practice, we found that periodically changing the method of choosing $g_{k+1}(x, y)$ after a few iterations works better than using any one method for all iterations.

## III. Experimental Results: Noise-Free Case

Figure 3(a) shows a computer-synthesized object resembling a sun having solar flares and bright and dark sunspots. The diameter of

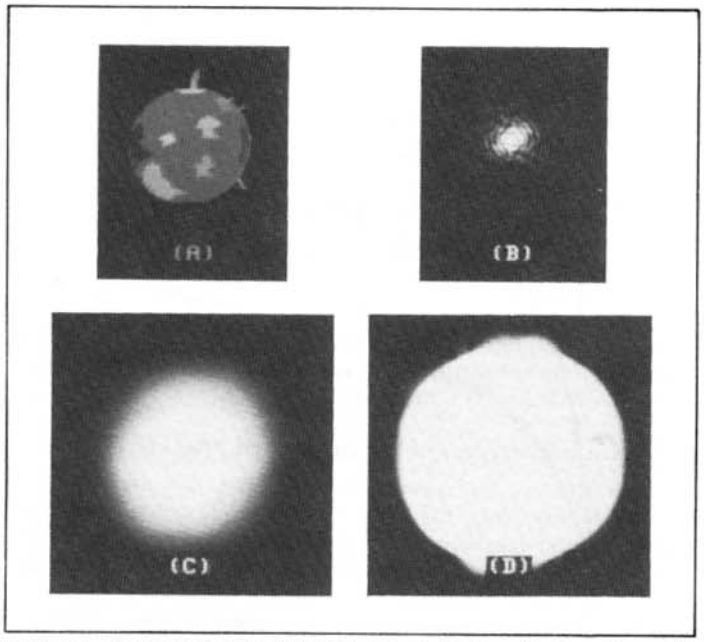


**Figure 3. (a) Sun object; (b) modulus of its Fourier transform; (c) autocorrelation; (d) autocorrelation, displayed at high intensity (overexposed).**

the sun's disc is 52 pixels in a field of 128 x 128 pixels. Figure 3(b) shows the modulus of the Fourier transform of the sun object. It is highly peaked at zero spatial frequency (u = v = 0), as is usually the case for Fourier transforms of real, non-negative functions. The periodic circular fringes seen in Figure 3(b) are due to the basically circular shape of the object. The nulls of these fringes are equivalent to the nulls of the visibility function as seen through the Michelson stellar interferometer, which was used in the first calculations of stellar diameters.[15] Both Figures 3(c) and 3(d) show the autocorrelation of the sun object, displayed at different intensities [Figure 3(d) is highly overexposed in order to bring out the edges of the autocorrelation]. From the autocorrelation, the circular shape and the diameter of the object are obvious, and the existence of the largest solar flare might be inferred; but the structure of the sunspots could not be guessed.

Figure 4 shows the results of two tests of the iterative approach using the Fourier modulus of the sun object. Figure 4(a) shows the initial estimate of the object used for the first test: a 64 x 64 square of uniformly distributed random numbers imbedded in the 128 x 128 array (only 80 x 80 pixels are shown). Figures 4(b)–(f) show the reconstruction results after 20 ($E_0$ = 0.117), 100 ($E_0$ = 0.068), 230 ($E_0$ = 0.042), 330 ($E_0$ = 0.024), and 600 iterations ($E_0$ = 0.0055), respectively. Figure 4(g) shows the initial estimate of the object for the second test: a circle of random numbers.

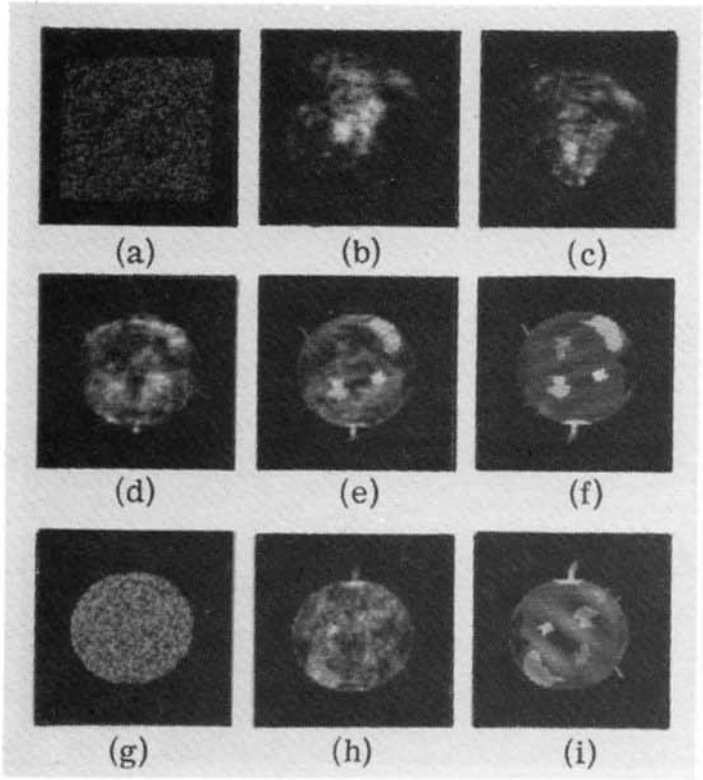


**Figure 4. (a) Initial estimate of the object (first test); (b)-(f) reconstruction results—number of iterations: (b) 20, (c) 100, (d) 230, (e) 330, (f) 600; (g) initial estimate of the object (second test); (h)-(i) reconstruction results—number of iterations: (h) 20, (i) 215.**

Figures 4(h) and 4(i) show the reconstruction results of the second test after 20 iterations ($E_0$ = 0.051) and 215 iterations ($E_0$ = 0.019), respectively. In this case and the cases that follow, for reasons of economy the iterations were halted before the error was driven to zero.

The reconstruction method was also subjected to a blind test with noise-free Fourier modulus data supplied by B. L. McGlamery (Visibility Laboratory, Scripps Institution of Oceanography, U. C. San Diego). The 128 x 128 Fourier modulus array provided by McGlamery is shown in Figure 5(a) and the autocorrelation computed from it in Figure 5(b). Figure 6(a) shows the initial estimate of the object, and the reconstruction results after 10, 60, 200, 240, 280, and 400 iterations are shown in Figures 6(b) through 6(g), respectively. Using a different initial

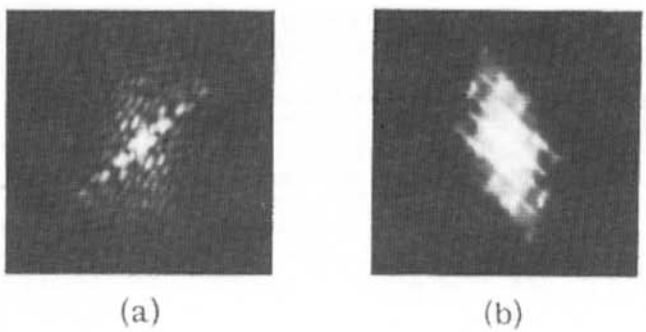


**Figure 5. (a) Noise-free Fourier modulus data; (b) noise-free autocorrelation.**

estimate, the second reconstruction result shown in Figure 6(h) was obtained. The rms error $E_0$ is 0.073 and 0.051 for the images shown in Figures 6(g) and 6(h), respectively. Only after these

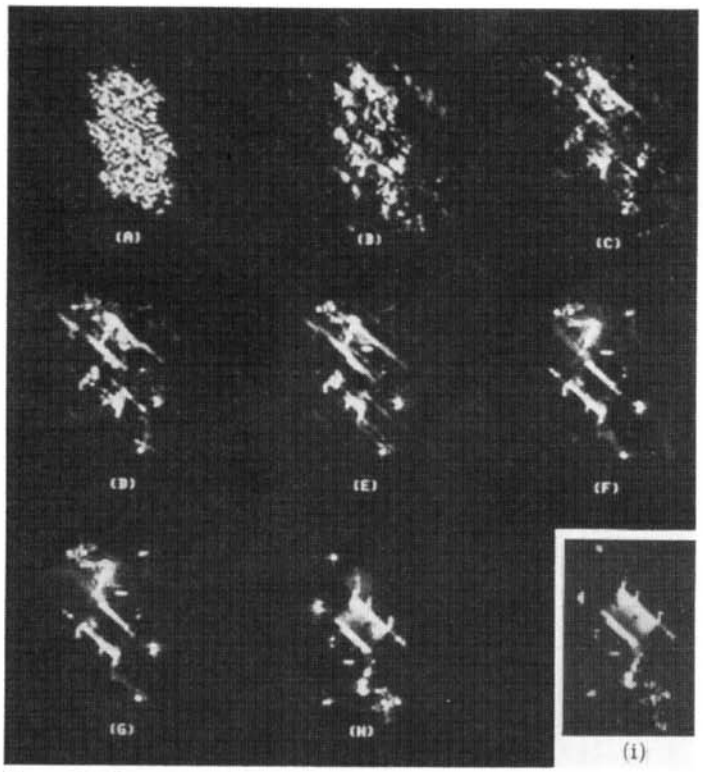


**Figure 6. Reconstructions from noise-free Fourier modulus data. (a) Initial estimate of the object (first test); (b)-(g) reconstruction results—number of iterations: (b) 10, (c) 60, (d) 200, (e) 240, (f) 280, (g) 400; (h) reconstruction result (second test); (i) the object.**

results were obtained did McGlamery send a picture of the object, which is shown in Figure 6(i).

Comparing Figures 4(f) and 4(i) with Figure 3(a) and comparing Figures 6(g) and 6(h) with Figure 6(i), we see that the reconstruction results differ very little from the respective original objects. Note that inverted solutions are allowed, since $|\mathcal{F}\{f(-x, -y)\}| = |\mathcal{F}\{f(x, y)\}|$.

These results are very significant because (1) they demonstrate a practical method for finding solutions from the Fourier modulus and (2) they suggest that the uniqueness problem is not a serious limitation for complicated two-dimensional objects (despite the theory which shows that the solution is not generally unique[16]).

## IV. Simulation of the Speckle Interferometer Process

Another blind test of the reconstruction method was performed on data that is a realistic simulation of the stellar speckle interferometer (or speckle imaging) process. In this section, the simulation of the speckle data, which was performed by McGlamery, is briefly described (it is described by McGlamery[17] in detail).

The object used was a lower-resolution version of the object shown in Figure 6(i). 320 different point spread functions (PSFs) $s_m(x, y)$, $m = 1, \ldots, 320$, were computed from phase arrays representing the effects of atmospheric turbulence. After proper scaling, 160 blurred images, $d_m(x, y)$, were computed by convolution of the undegraded object, $f(x, y)$, with the PSFs:

$$d_m(x, y) = f(x, y) * s_m(x, y)$$
$$= \mathcal{F}^{-1}\{F(u, v) \cdot S_m(u, v)\}, \; m = 1, \ldots, 160 \tag{8}$$

Making realistic assumptions about the object and the sensor system, including the spectral power falling on the object, the reflectivity of the object, the distance to the object, the transmittance of the atmosphere, the diameter of the telescope aperture (1.2 m), the transmittance of the optical system, the spectral sensitivity of the detector, and the exposure time (5 msec), the degraded images were converted into photon counts, which were then subjected to a Poisson noise process. Each pixel of $d_m(x, y)$ was replaced with a noise sample drawn from a Poisson noise distribution with mean and variance equal to the photon count for the pixel. The result is the noisy degraded images $i_m(x, y)$. To simulate the speckle processing, the square of the modulus of the Fourier transform

$$|I_m(u, v)|^2 = |\mathcal{F}\{i_m(x, y)\}|^2 \tag{9}$$

of each of the noisy degraded images was taken, and the sum over all of the frames was computed. That sum was then divided by the sum of the squares of the moduli of the Fourier transforms of the second 160 PSFs. This division provides an approximate compensation for the MTF of the speckle process.

The data provided by McGlamery was the square root of the result:

$$R(u, v) = \left[ \frac{\sum_{m=1}^{160} |I_m(u, v)|^2}{\sum_{m=161}^{320} |S_m(u, v)|^2} \right]^{1/2} \tag{10}$$

$R(u, v)$ is the simulation of the data that would be provided by the speckle interferometer process. It is a noise-degraded approximation of the undegraded Fourier modulus, $|F(u, v)|$.

## V. Characteristics of the Simulated Speckle Data

The data $R(u, v)$ was provided in a 256 x 256 array and is shown in Figure 7(a). It is bounded by a circle due to the shape of the telescope aperture. Although $R(u,v)$ is of size 256 x 256, it is of somewhat lower resolution (i.e., lower maximum spatial

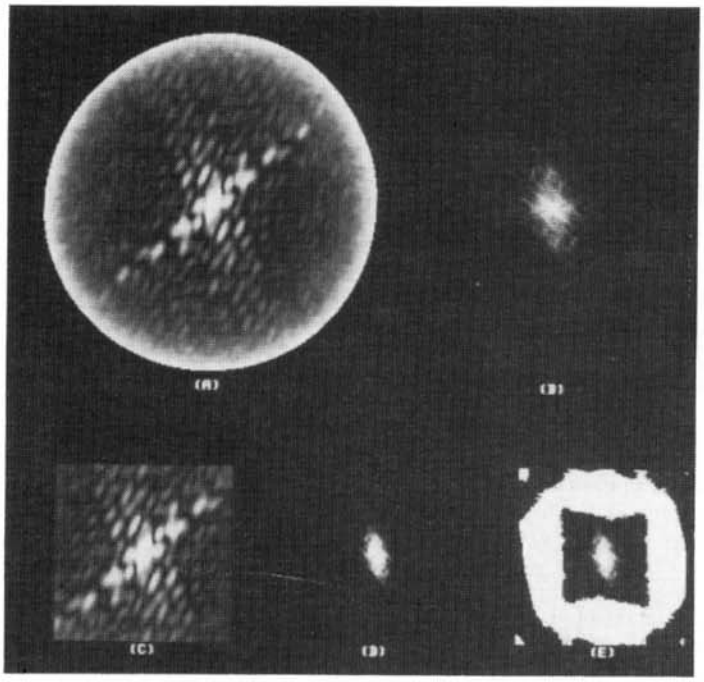


**Figure 7. Simulated speckle data. (a) 256 x 256 array R(u, v); (b) degraded autocorrelation computed from (a); (c) 128 x 128 subarray of R(u, v); (d) degraded autocorrelation computed from (c); (e) same as (d), with negative values shown as bright areas.**

frequency) that the Fourier modulus data shown in Figure 5(a). This results from the fact that R(u, v) was sampled at more than twice the rate of the noise-free |F(u, v)|. A degraded autocorrelation is given by $\mathcal{F}^{-1}[|R(u, v)|^2]$, which is an approximation to the autocorrelation of the undegraded object. Figure 7(b) shows the degraded autocorrelation computed from R(u, v). The degraded autocorrelation is dominated by a pattern of concentric circles that bears no relationship to the undegraded object. The pattern of concentric circles is an artifact that arises from a noise component of R(u, v) that is heavily concentrated in an annulus at the perimeter of the circle [which can be seen in Figure 7(a)].

The source of the annulus of noise is as follows. Included in the numerator of Eq. (10) are noise terms that are non-zero for all spatial frequencies. However, the denominator of Eq. (10) goes to zero at $f_{co}$, the cut-off spatial frequency of the telescope, as shown in Figure 8; consequently, R(u, v) is large near $f_{co}$. Had the

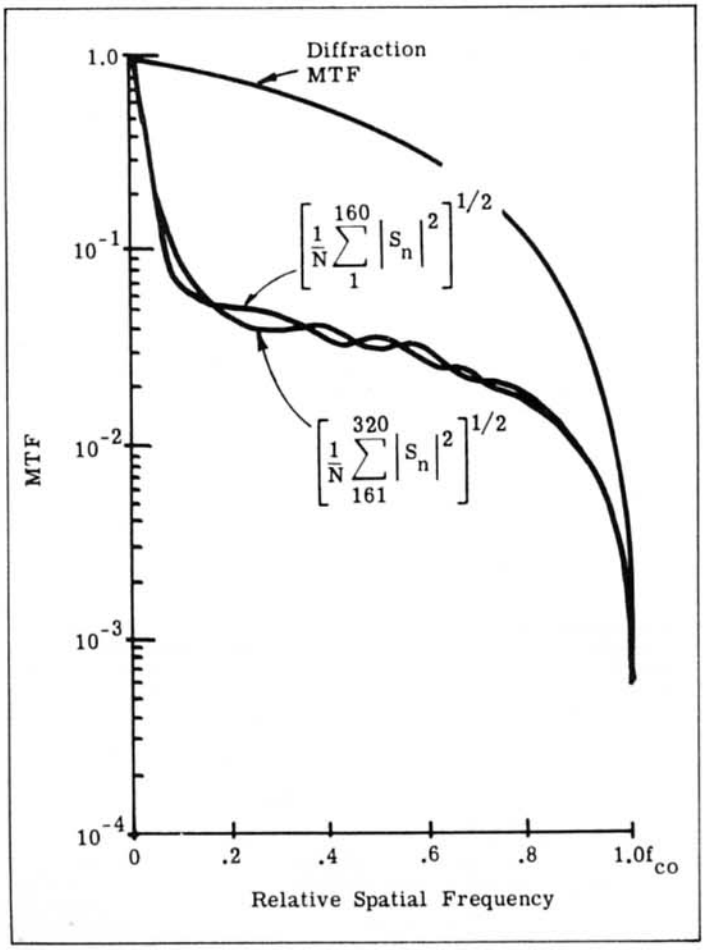


**Figure 8. Modulation transfer functions: of the telescope aperture (uppermost curve); of the actual speckle process (second curve); of a second speckle process, used to approximately compensate for the actual speckle process (third curve). (From Figure 2 of Ref. 17).**

simulation been performed including the noise process in the denominator of Eq. (10), then the strong annulus of noise may not have occurred.

For spatial frequencies exceeding $f_{co}/2$, the noise dominates (u, v) as can be seen from Figure 9. At $f_{co}/2$ the signal-to-noise ratio is about 2:1. Consequently, R(u, v) for spatial frequencies above $f_{co}/2$ is not useful for image reconstruction. For this reason, we discarded the values of R(u, v) for the higher spatial frequencies, and processed the data at half resolution using our method. Figure 7(c) shows the 128 x 128 portion of R(u, v) used for our reconstruction experiments. Figure 7(d) shows the degraded autocorrelation computed from the 128 x 128 version of R(u, v). The degraded

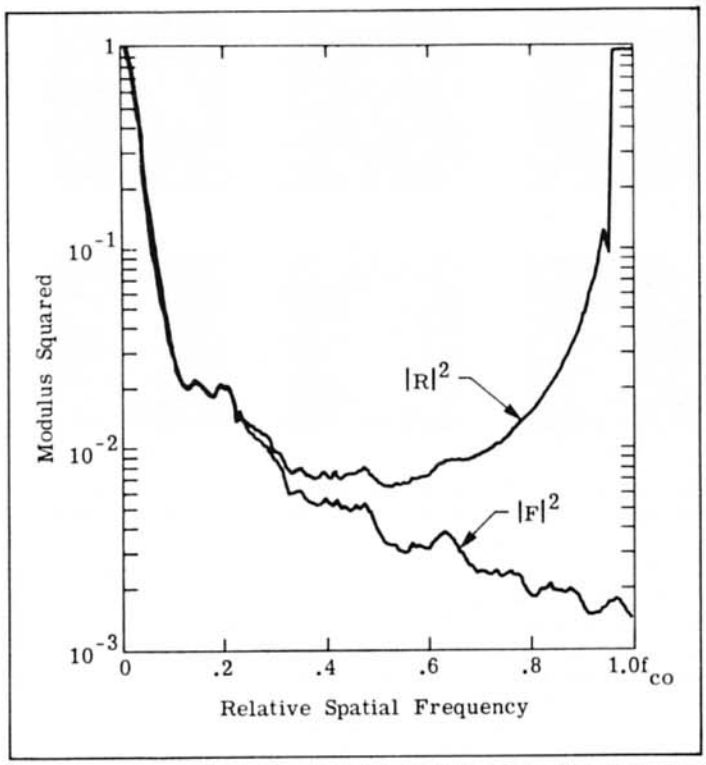


**Figure 9. Square of Fourier modulus data from simulated speckle process $|R|^2$; and square of Fourier modulus of object, $|F|^2$. (From Figure 3 of Ref. 17).**

autocorrelation is displayed at half the size as before, since it is at half the resolution. The pattern of concentric circles in the autocorrelation is gone; however, the level of noise in the 128 x 128 portion of R(u, v) is still quite large. An indication of this is that the autocorrelation computed from the 128 x 128 R(u, v) has areas of negative values. This cannot be seen from Figure 7(d) since the negative values were arbitrarily set to zero for the display of that autocorrelation. Figure 7(e) shows the same autocorrelation, except that in this case, the negative values were displayed as bright areas, showing the extent of the area with negative values. It can easily be shown that an autocorrelation with negative values can arise only from an object with negative values. That is, there can be no non-negative (physical) object that would give rise to a Fourier modulus equal to R(u, v). Nevertheless, as will be shown in the next section, our reconstruction method, which relies on the non-negativity of the solution, finds a solution that has a minimum amount of negative values; in doing so, it reconstructs an image that contains much useful information about the original object.

## VI. Reconstruction Results from the Noisy Modulus Data

The reconstruction results from the 128 x 128 R(u, v) are shown in Figure 10. Three tests of the method were performed, each with a different initial estimate of the object. The three reconstructed images are shown in Figure 10(a)–(c), having rms errors $E_0$ of 0.078, 0.091, and 0.073, respectively. For comparison, Figure 10(d) shows the undegraded object (provided by McGlamery after the tests were completed) displayed at the same bandwidth (resolution) at which the reconstruction was performed on R(u, v). Also for comparison, two realizations of the noisy, degraded images, given by $i_m(x, y)$ in Section IV, are shown in Figures 10(e) and (f). These correspond to the short-exposure images that would ordinarily be seen through a telescope.

In this case with noise present, the solution is no longer unique, as seen by comparing the three reconstructed images in Figures 10(a)–(c) with one another. Nevertheless, the three reconstructed

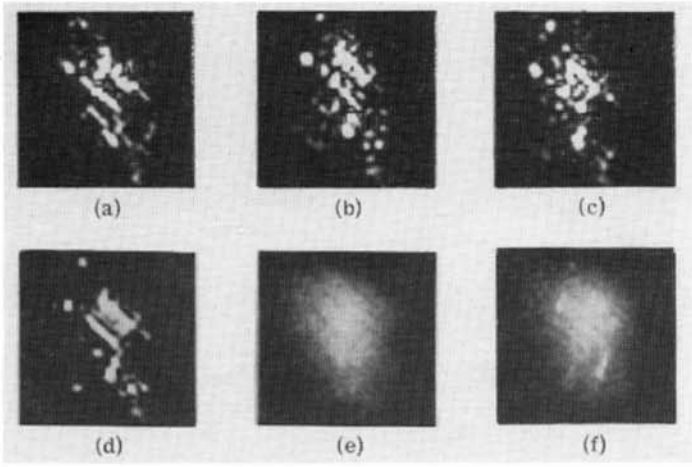


**Figure 10. (a)-(c) Images reconstructed from simulated speckle data; (d) original object; (e)-(f) examples of simulated short-exposure images.**

images do share a number of common features, and they correlate well with the original object. Most important, the reconstructed images contain significantly more information than the images that would ordinarily be obtained through a telescope.

## VII. Discussion and Conclusions

We have shown that our image reconstruction method is successful in reconstructing images from speckle interferometer data. Still better performance is possible if (a) a larger telescope is used (giving better photon statistics), (b) a greater number of short-exposure photographs is used to compute the Fourier modulus data R(u, v), and (c) the Fourier modulus data is preprocessed to increase the signal-to-noise ratio. An example of preprocessing R(u, v) is to subtract out a particular constant noise term which is described by Goodman and Belsher;[18] another is to weight it, emphasizing the spatial frequencies where the signal-to-noise ratio is higher (i.e., the lower spatial frequencies). In addition, possibilities exist for combining the various solutions that are generated to form a single best estimate of the object, for example, by forming the sum or the product of all the solutions or by extracting common features. The results shown here represent only a first-try effort, and further research is expected to yield improved results.

We have demonstrated an iterative approach to the reconstruction of an object from the modulus of its Fourier transform, and have shown it to succeed even in the presence of large amounts of noise. This method can be expected to reconstruct images with resolution many times better than what is normally allowed by the turbulent atmosphere, using data from a speckle (or other) interferometer. Using the Fast Fourier Transform (FFT), the iterations are relatively fast, making it practical for use on two-dimensional images of large space-bandwidth product. Alternative approaches for performing the iterative computations may also be developed using electro-optical techniques.

This work was performed under an ERIM internal research program.

## References

1. R. H. T. Bates and P. T. Gough, "New Outlook on Processing Radiation Received from Objects Viewed Through Randomly Fluctuating Media," IEEE Trans. Comput. *C-24*, 449–456 (1975).
2. R. Hanbury Brown and R. Q. Twiss, "Correlation Between Photons in Two Coherent Beams of Light," Nature *177*, 27–29 (1956).
3. A. Labeyrie, "Attainment of Diffraction Limited Resolution in Large Telescopes by Fourier Analysing Speckle Patterns in Star Images," Astron. & Astrophys. *6*, 85–87 (1970); D. Y. Gezari, A. Labeyrie, and R. V. Stachnik, "Speckle Interferometry: Diffraction-Limited Measurements of Nine Stars with the 200-inch Telescope," Astrophys. J. Lett. *173*, L1–L5 (1972).
4. D. G. Currie, S. L. Knapp, and K. M. Liewer, "Four Stellar-Diameter Measurements by a New Technique: Amplitude Interferometry," Astrophys. J. *187*, 131–44 (1974).
5. E. Wolf, "Is a Complete Determination of the Energy Spectrum of Light Possible from Measurements of the Degree of Coherence?," Proc. Phys. Soc. (London) *80*, 1269–72 (1962).
6. A. Walther, "The Question of Phase Retrieval in Optics," Optica Acta *10*, 41–49 (1963).
7. H. M. Nussenzveig, "Phase Problem in Coherence Theory," J. Math. Phys. *8*, 561–72 (1967).
8. D. Kohler and L. Mandel, "Source Reconstruction from the Modulus of the Correlation Function: A Practical Approach to the Phase Problem of Optical Coherence Theory," J. Opt. Soc. Am. *63*, 126–134 (1973).
9. B. R. Frieden and D. G. Currie, "On Unfolding the Autocorrelation Function," J. Opt. Soc. Am. *66*, 1111 (1976) (Abstract).
10. J. R. Fienup, "Reconstruction of an Object from the Modulus of Its Fourier Transform," Opt. Lett. *3*, 27–29, (1978).
11. R. W. Gerchberg and W. O. Saxton, "A Practical Algorithm for the Determination of Phase from Image and Diffraction Plane Pictures," Optik *35*, 237–46 (1972).
12. N. C. Gallagher and B. Liu, "Method for Computing Kinoforms that Reduces Image Reconstruction Error," Appl. Opt. *12*, 2328–35 (1973).
13. J. R. Fienup, "Reduction of Quantization Noise in Kinoforms and Computer-Generated Holograms," J. Opt. Soc. Am. *64*, 1395 (1974) (Abstract).
14. J. R. Fienup, "Improved Synthesis and Computational Methods for Computer-Generated Holograms," Ph.D. thesis, Stanford University, May 1975 (University Microfilms No. 75-25523), Chapter 5.
15. A. A. Michelson and F. G. Pease, "Measurement of the Diameter of Alpha Orionis with the Interferometer," Astrophys. J. *53*, 249–59 (1921).
16. P. Roman and A. S. Marathay, "Analyticity and Phase Retrieval," Il Nuovo Cim. *30*, 1452–63 (1963).
17. B. L. McGlamery, "Summary of Processing for Speckle Simulations," Private communication, March 17, 1978.
18. J. W. Goodman and J. F. Belsher, "Fundamental Limitations in Linearly Invariant Restoration of Atmospherically Degraded Images," Proc. of the SPIE *75*, *Imaging Through the Atmosphere*, p. 141 (March 1976).